PNAS RESEARCH ARTICLE | NEUROSCIENCE OPEN ACCESS

Brain state limits propagation of neural signals in laminar cortical circuits

Natasha Kharas[a,c], Ariana Andrei[a], Samantha R. Debes[a], and Valentin Dragoi[a,b,1]

Edited by David Fitzpatrick, Max Planck Florida Institute for Neuroscience, Jupiter, FL; received March 4, 2021; accepted May 18, 2022 by Editorial Board Member Thomas D. Albright

Our perception of the environment relies on the efficient propagation of neural signals across cortical networks. During the time course of a day, neural responses fluctuate dramatically as the state of the brain changes to possibly influence how electrical signals propagate across neural circuits. Despite the importance of this issue, how patterns of spiking activity propagate within neuronal circuits in different brain states remains unknown. Here, we used multielectrode laminar arrays to reveal that brain state strongly modulates the propagation of neural activity across the layers of early visual cortex (V1). We optogenetically induced synchronized state transitions within a group of neurons and examined how far electrical signals travel during wakefulness and rest. Although optogenetic stimulation elicits stronger neural responses during wakefulness relative to rest, signals propagate only weakly across the cortical column during wakefulness, and the extent of spread is inversely related to arousal level. In contrast, the light-induced population activity vigorously propagates throughout the entire cortical column during rest, even when neurons are in a desynchronized wake-like state prior to light stimulation. Mechanistically, the influence of global brain state on the propagation of spiking activity across laminar circuits can be explained by state-dependent changes in the coupling between neurons. Our results impose constraints on the conclusions of causal manipulation studies attempting to influence neural function and behavior, as well as on previous computational models of perception assuming robust signal propagation across cortical layers and areas.

cortical column | brain state | neural circuits | optogenetics | visual cortex

Significance

Brain state fluctuates throughout the course of the day. Whether and how these fluctuations impact signal propagation in the brain remains unknown. Here, we used optogenetic stimulation during different brain states to show that the coupling between neurons modulates the spread of signals across cortical circuits in a state-dependent manner. Our results indicate that brain state influences how far electrical signals travel in neocortex and suggest a revision of computational models relying on robust signal propagation across neural networks.

The extent and accuracy with which neural signals propagate within and across neural circuits play a critical role in shaping behavior and cognition. One key variable that could potentially influence signal propagation across neural networks is global brain state (1–4). Indeed, during the time course of a day, the state of the brain undergoes dramatic changes from wakefulness to drowsiness and sleep (3, 5–7). Multiple lines of evidence in rodents and monkeys have shown that distinct brain states are associated with specific changes in neural responses (2–4, 8). Neurons strongly respond during wakefulness when animals are in an aroused state, and responses diminish during drowsiness and sleep (6, 9–11). However, despite significant progress in our understanding of state-dependent sensory coding across neural circuits (2–5, 8, 12, 13), the influence of brain state on the propagation of electrical signals remains unknown.

The cortical column constitutes an ideal locus to examine the propagation of neural signals. For over a century, neuroscientists have observed remarkable regularity in the cortical microarchitecture: Clusters of cells are synaptically connected to form small columns orthogonal to the cortical surface (14, 15). These microcolumns constitute the elementary functional units of cortical circuitry (16) and consist of distinct layers that each contain a characteristic distribution of cell types and connections with other layers (15, 17–19). Understanding how neural signals propagate across laminar circuits would greatly contribute to deciphering the functional principles of cortical column operation.

In principle, the strong intracortical connections within and between cortical layers (17–20) imply that signals emitted by individual neurons would vigorously propagate across the entire microcolumn. Indeed, during wakefulness, the input granular (G) cortical layers relay stimulus information to the output supragranular (SG) layers, which send feedforward projections to downstream areas (18, 20). Furthermore, neurons in SG layers project back to infragranular (IG) layers, which in turn project to granular layers; hence, signals are circulated across the entire microcolumn (17, 18). Thus, from a theoretical standpoint, it can be argued that electrical signals are robustly transmitted during wakefulness across cortical layers to contribute to perception and cognition. In reality, how robustly signals travel across layers in different states of wakefulness, and especially

Author affiliations: [a]Department of Neurobiology and Anatomy, McGovern Medical School, University of Texas, Houston, Houston, TX 77030; [b]Department of Electrical and Computer Engineering, Rice University, Houston, TX 77005; and [c]Department of Neurosurgery, NewYork-Presbyterian Weill Cornell Medical Center, New York, NY 10021

Author contributions: V.D. designed research; N.K., A.A., and S.R.D. performed research; N.K. analyzed data; and N.K. and V.D. wrote the paper.

The authors declare no competing interest.

This article is a PNAS Direct Submission. D.F. is a guest editor invited by the Editorial Board.

[1]To whom correspondence may be addressed. Email: v.dragoi@uth.tmc.edu.

This article contains supporting information online at http://www.pnas.org/lookup/suppl/doi:10.1073/pnas.2104192119/-/DCSupplemental.

Published July 18, 2022.

when the state of the brain undergoes dramatic changes, such as during drowsiness and sleep, remains unknown.

Previous studies were unable to address these issues due to inherent restrictions of techniques such as in vitro slice recordings [e.g., (21)] and in vivo recordings during anesthesia (6, 10, 22) that severely limit the behavioral repertoire and hence the interpretation of cortical dynamics across laminar circuits. Even studies focused on in vivo laminar recordings failed to investigate state-dependent signal propagation across cortical layers (23–25). Here, we examined the propagation of neural signals across the cortical column in different brain states using multielectrode laminar arrays. We discovered that the global brain state strongly modulates the propagation of neural activity across the layers of the early visual cortex (area V1). We optogenetically activated specific cell populations during wakefulness to find that even though the elicited neural signals were stronger than those during rest, they propagated to other layers only weakly. Further, arousal was inversely related to the extent of signal spread. In contrast, the light-induced activity of the same neural population robustly propagated throughout the entire cortical column during rest, even when neurons were in a desynchronized wake-like state prior to light stimulation. The differential propagation of electrical signals in different brain states can be explained by state-dependent changes in the degree of coupling between individual neurons and their local population. Our results impose constraints on the conclusions of causal manipulation studies attempting to influence neural function and behavior, as well as on previous computational models of perception assuming robust signal propagation across cortical layers and areas.

Results

State-Dependent Dynamics of Laminar Population Activity. We first examined the spiking activity of 1,407 cells across the layers of V1 of three behaving rhesus macaques using 16- and 24-channel linear array microelectrodes (25, 26). These arrays allowed us to record multiple neurons with largely overlapping receptive fields across the entire depth of cortex (Fig. 1 and *SI Appendix*, Figs. S1 and S2). Neural responses were recorded in different brain states while animals performed a fixation or a behavioral task (see *Methods*) and during 20 minutes (min) of rest. To avoid stimulus-induced confounds, we measured neurons' responses in a 1,000-ms interval in the absence of external visual stimulation in wakefulness conditions of passive fixation and during the blank period of a behavioral task, and during periods of rest (Fig. 1*A*–*C*; 17,534 trials during wakefulness and 9,110 pseudotrials of identical length during rest). We controlled the lights in the room and monitor brightness such that the experimental setup was identical in all three conditions. As revealed by analyzing local field potentials (LFPs), wakefulness was associated with increased high-frequency LFP power (30 to 80 Hz) and decreased low-frequency power (1 to 20 Hz), while high-frequency power was decreased and low-frequency power was increased during rest ((1, 5) Fig. 1*A*–*C*). As animals rested with their eyes closed, prominent On-Off transitions occurred synchronously across cortical layers (Fig. 1*C*). However, during wakefulness, in agreement with previous results in sensory cortices in which neuronal activity was measured at multiple sites along the cortical surface (1, 2, 4), the population of cells emitted action potentials in a desynchronized manner (Fig. 1*A* and *B*).

The dynamics of neuronal responses across the cell population ($n = 95$ sessions) were characterized by counting spikes in 10-ms bins. Overall, firing rates were elevated when the animal performed a task compared to rest, but not when monkeys fixated on the center of a computer screen (*SI Appendix*, Fig. S12*A*). Mirroring the frequent On-Off transitions observed during rest, there was significantly higher variability (Standard deviation, SD; *SI Appendix*, Figs. S12*B* and S14) and higher coefficient of variation (SD divided by mean; *SI Appendix*, Fig. S12*C*) in the rest condition compared to wakefulness. We further used a two-state Hidden Markov Model (HMM; (23, 27) Fig. 1*D*), which has a one-dimensional, latent variable representing an unobserved population state switching between the On and Off states (23). We fitted the HMM to summed multiple single-unit spiking data across layers to transform the spike-count data into On and Off episodes under the assumption that spikes are generated via a Poisson process (Fig. 1*D* and *E* and *SI Appendix*, Fig. S3*A*). While On and Off episodes resembling the Up and Down states routinely found during anesthesia and slow-wave sleep (1–3, 28) were often identified during rest, they were scarce during wakefulness regardless of whether animals performed a behavioral task or simply fixated on a computer screen (Fig. 1*A*–*C* and *SI Appendix*, Fig. S4). Across sessions, columnar synchrony (calculated as transition rate between On and Off states derived from HMM) was significantly greater in rest compared to wakefulness (Fig. 1*F* and *G*; χ^2 test, $P < 0.0001$). In those rare wakefulness trials in which we observed On-Off transitions, we found that fluctuations in pupil size, a measure of global arousal, was related to the probability of occurrence of On and Off states—on a trial-by-trial basis, there was a negative correlation between pupil size and rate of On-Off transitions (Fig. 1*H*; Pearson correlation coefficient, $R = -0.10$, $P < 0.05$); that is, high arousal (larger pupil) decreases the rate of On-Off synchrony during wakefulness, whereas low arousal (smaller pupil) increases it. In contrast, rest was accompanied by significantly higher On-Off transition rates of 12 to 26 transitions/s (Fig. 1*C* and *G*). These results were also found throughout the layers of V1 (Fig. 1*I*–*K* and *SI Appendix*, Figs. S4, S6*A*, and S8*A*); similar results were found in area V4 (*SI Appendix*, Figs. S1, S3*B*, S4, S5, S6*B*, S7, and S8*B* describe similar dynamics in V4).

Neuron firing rates in the On state were significantly higher than those in the Off state across all three behavioral conditions in both V1 and V4 areas ($P < 0.05$, Wilcoxon rank sum test for each comparison). During wakefulness, the proportions of time spent in the On or Off states were relatively equal (*SI Appendix*, Fig. S15, *Left*; $P > 0.05$, Wilcoxon rank sum test). In general, we found that neuronal populations that were in an On state at the beginning of a trial were more likely to spend more time in the On state during that trial (this was also true for the Off states). Furthermore, the proportion of time spent in the On and Off states did not vary based on changes in the animal's arousal (*SI Appendix*, Fig. S15, *Right*; $P > 0.05$, χ^2 test). Lastly, during rest, we found a higher likelihood of Off states compared to wakefulness ($P < 0.05$, χ^2 test).

Brain State Modulates the Propagation of Optogenetically Induced Neural Signals. We examined whether the propagation of cortical signals depends on global brain state. We directly investigated this issue by optogenetically inducing synchronized On-Off transitions in a subset of neurons while measuring the propagation of induced signals to adjacent neurons across the cortical column during wakefulness and rest (Fig. 2*A*). This was done by injecting lentivirus with an alpha-Ca(2+)/calmodulin-dependent protein kinase II (α-CaMKII) promoter to express Channelrhodopsin-2 (*ChR2*) in excitatory V1 neurons across the cortical column and then optically stimulating a subset of

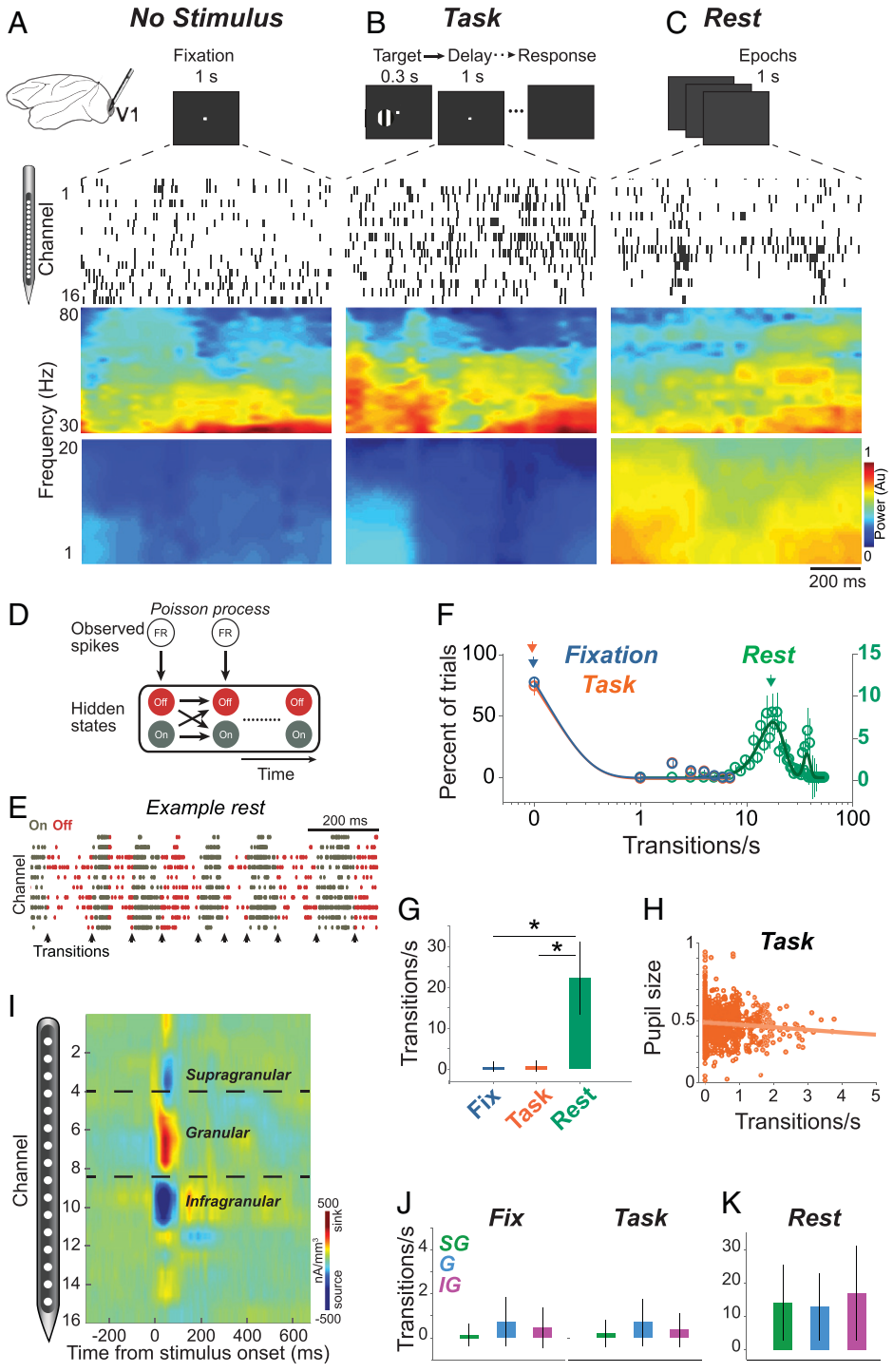

Fig. 1. Dynamics of cortical population activity during wakefulness and rest across cortical layers. (*A*) Schematic representation of electrophysiological recordings using laminar probes in V1 (*Top*). Diagram of "no stimulus" condition: Animals were trained to passively fixate on the center of a computer screen for 1 s. Raster plots represent single units recorded across 16 channels for example time epochs. The spectrograms on the *Bottom* represent the corresponding low- (1- to 20-Hz) and high- (30- to 80-Hz) frequency LFP power. (*B*) Schematic representation of "task" condition (*Top*). Animals were trained to report whether a low-contrast visual stimulus was present on a computer screen. Example neuronal activity (*Middle*) and LFP (*Bottom*) for the 1-s interval (delay) following stimulus presentation. (*C*) Animals rested for 20 to 40 min (*Top*). Example neuronal activity (*Middle*) and LFP (*Bottom*) during a 1-s rest epoch. (*D*) Schematic of a two-state HMM to elucidate hidden states (On and Off) from population firing. (*E*) Example neuronal activity colored as On and Off states as predicted by the model; transitions between On and Off states are indicated by arrows. (*F*) Histograms of rate of transition between On and Off states during fixation, task, and rest in V1. Arrows indicate medians, and error bars represent SEM. (*G*) Transitions/s plotted as mean and standard deviation (SD) during fixation, task, and rest in V1 (transition rate in rest versus fixation and task, $*P < 0.0001$, Chi(X)^2 test, $n = 27$ sessions). (*H*) Scatter plot of mean pupil size and rate of transitions on a trial-by-trial basis (V1, $R = -0.10$, $P < 0.05$, Pearson correlation, $n = 815$ trials). (*I*) CSD analysis to identify supragranular (SG), granular (G), and IG layers by detecting the polarity inversion accompanied by the sink-source configuration at the base of the granular (G) layer. Example current sink (shown as red) represents the granular layer and spans ~400 μm. (*J*) Rate of transition between On and Off states in each cortical layer during fixation and task within V1 (during fixation, layer pairs of SG versus IG, SG versus G, and G versus IG, $P > 0.05$, ChiX^2 test, $n = 13$ sessions; during task, layer pairs compared, $P > 0.05$, X^2 test, $n = 13$ sessions). Bars represent mean, and error bars represent SD. (*K*) Rate of transition between On and Off states in each cortical layer during rest within V1 (layer pairs of SG versus IG, SG versus G, and G versus IG in V1, $n = 12$ sessions, $P > 0.05$, X^2 test). Bars represent mean, and error bars represent SEM.

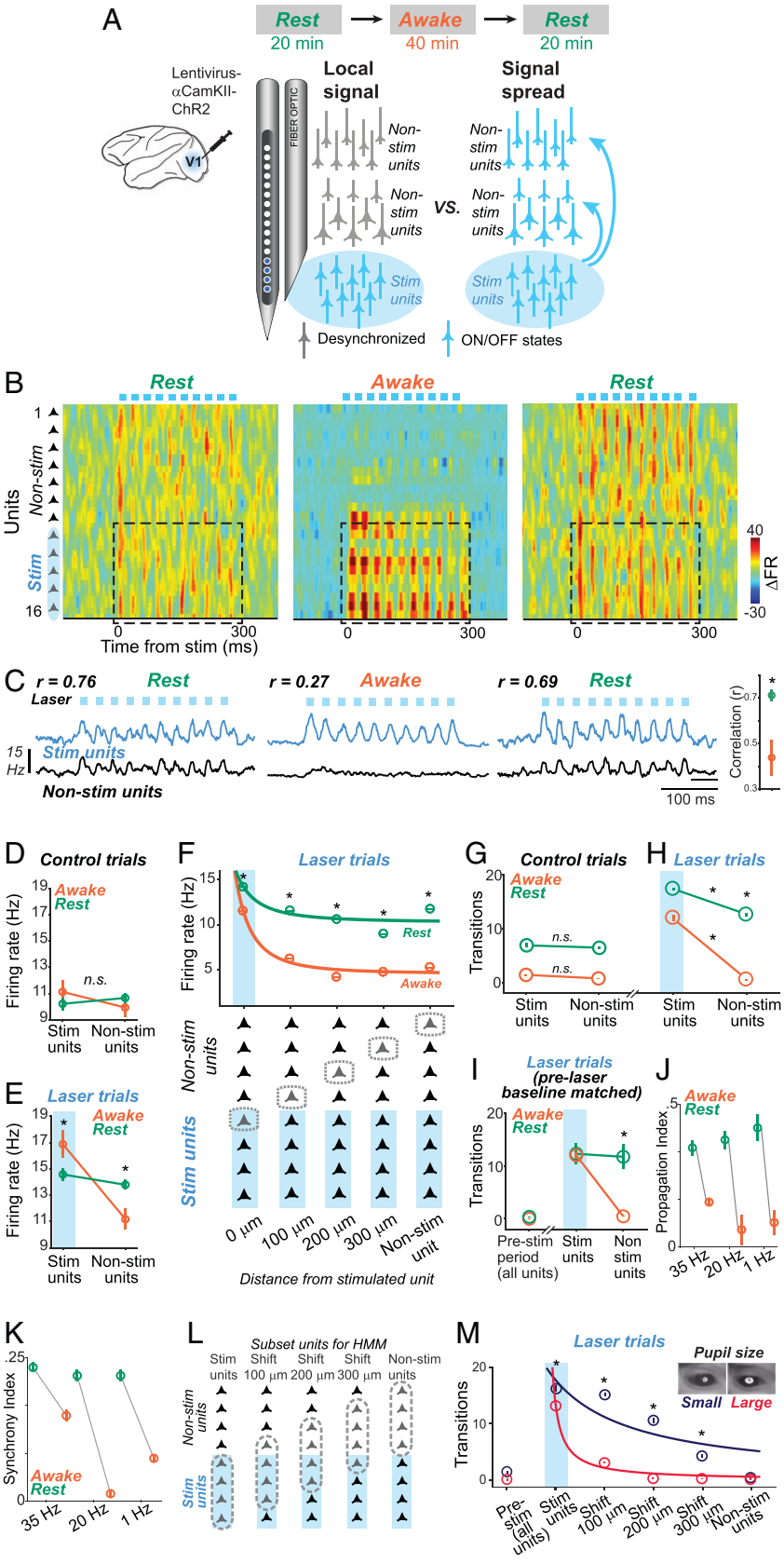

Fig. 2. State-dependent propagation of cortical spiking activity. (*A*) *Top*: Diagram of the experimental protocol: 20 min of rest was followed by 40 min of wakefulness (fixation task) and then another 20-min period of rest. Schematic of two scenarios: Induced signal remains local at the light stimulation site (*Left*), and induced signal spreads across the entire column (*Right*). Area V1 was injected with ChR2 so as to optogenetically induce synchronous On-Off states. (*B*) Heat maps represent the difference in firing rates (ΔFR) between stimulated and control trials across all units in three recording sessions performed (Rest-Awake-Rest). Optogenetically induced On (high FR) and Off (low FR) states in units are indicated by dashed box. (*C*) Mean population firing rates represented for optogenetically stimulated and nonstimulated units in example sessions (wake versus rest, $*P < 0.01$, Wilcoxon rank sum test). Pearson correlation coefficient (r) computed between mean firing rates of stimulated and nonstimulated units (*Right*: awake versus rest, $*P < 0.001$, Wilcoxon rank sum test, $n = 12$ sessions). Bars represent SEM. (*D* and *E*) Mean firing rates of stimulated and nonstimulated units during wakefulness and rest in control (*D*) and laser (*E*) trials (laser trials, awake versus rest stimulated units, $*P < 0.001$; awake condition, stimulated versus nonstimulated units, $*P < 0.001$; Wilcoxon rank sum test, $n = 12$ sessions, 35-Hz stimulation). Bars represent SEM. (*F*) Mean firing rates of individual units, plotted as a function of distance from stimulated units, in rest compared to wakefulness (awake versus rest, $*P < 0.001$, Wilcoxon rank sum test, $n = 12$ sessions, 35-Hz stimulation). Bars represent SEM. Dashed boxes in the bottom panel represent the neuron analyzed. (*G* and *H*) Mean transition rate plotted as dots with SE for stimulated and nonstimulated units during wakefulness and rest in control (*G*) and laser (*H*) trials (laser trials: awake Stim versus awake Non-stim, $*P < 0.001$, χ^2 test, $n = 5$ sessions; laser trials: rest Stim versus rest Non-stim, $*P < 0.001$, χ^2 test, $n = 7$ sessions). Transition rate in nonstimulated units in rest compared to wakefulness in laser trials ($*P < 0.05$, χ^2 test, $n = 12$ sessions, 35-Hz stimulation). (*I*) Mean transition rate plotted as dots with SE in all units prestimulation, in stimulated and nonstimulated units in rest compared to wakefulness in laser trials (rest Non-stim versus awake Non-stim for desynchronized prestim condition; $*P < 0.001$, χ^2 test, $n = 7$ sessions, 35-Hz stimulation). (*J*) PI ($1/\Delta\ FR_{stim} - FR_{non\text{-}stim}$ in laser trials) plotted as dots with SE in rest compared to wakefulness in response to optogenetic stimulation at 35, 20, and 1 Hz (rest versus awake; $P < 0.001$, Wilcoxon rank sum test, $n = 11$ sessions). (*K*) SI ($1/\Delta$ On-Off transition rates in stim versus Non-stim units in laser trials) plotted as dots with SE in rest compared to wakefulness in response to optogenetic stimulation at 35, 20, and 1 Hz (rest versus awake, $P < 0.001$, Wilcoxon rank sum test, $n = 12$ sessions). (*L*) Schematic representation of the subset population of units analyzed (gray) with a sliding window of four units with step size of one unit (100 μm) moving away from stimulated units (blue highlight). (*M*) Mean transition rate plotted as dots with SE for subset of units analyzed as described in *L*. Transition rates plotted for wakefulness trials with larger-than-average pupil size (red) and smaller-than-average pupil size (blue) (small pupil versus large pupil; $*P < 0.01$, Wilcoxon rank sum test, $n = 4$ sessions, 35-Hz stimulation; 20-Hz stimulation yielded similar results). Non-stim, nonstimulated; *n.s.*, not significant, Stim, stimulated.

neurons ("stimulated units") while performing concurrent laminar recordings (stimulation and control trials were randomly interleaved; see *Methods*). We performed optogenetic activation in the 35-Hz frequency range while animals underwent a rest-awake cycle (Fig. 2*B*; i.e., either rest-awake-rest or awake-rest-awake sessions; see *Methods*). Light stimulation duration, frequency, and number of stimulation trials were identical across brain state conditions. We considered that signals had propagated effectively when both the stimulated and nonstimulated units exhibited an increase in firing rates due to laser pulses; in that case, we verified that the

optogenetic stimulation induced synchronous On-Off transitions across the entire cortical column (Fig. 2*A*). Hence, we measured both the firing rates and frequency of On-Off transitions induced by laser pulses to capture the extent of signal propagation in stimulated and nonstimulated units.

The 35-Hz optogenetic stimulation allowed us to transiently activate a subgroup of neurons using 10-ms light pulses presented for 300 ms while electrical activity was recorded across the entire depth of the cortex (Fig. 2*B*). We found both direct and indirect activation of neurons by light, indicating that optogenetic stimulation did spread across cells in the stimulated units (29, 30) (*SI Appendix*, Fig. S9). As expected, at the site of optogenetic stimulation, the population of neurons increased their firing rates in both brain states to elicit On and Off transitions (Fig. 2*B* and *C*). In control trials, the firing rates of stimulated and nonstimulated units were statistically indistinguishable and did not significantly differ between the awake and rest conditions (Fig. 2*D*; $P > 0.05$, Wilcoxon rank sum test for all comparisons). In laser trials, the light-induced neural responses of the stimulated units increased relative to control ($P < 0.01$, Wilcoxon rank sum test), and the evoked responses were stronger during wakefulness compared to rest (Stim units in Fig. 2*E*; $P < 0.001$, Wilcoxon rank sum test). However, the mean responses of nonstimulated units were significantly higher in the rest relative to the awake condition ($P < 0.001$, Wilcoxon rank sum test), where firing rates returned to the baseline values observed in control trials ($P > 0.05$; Fig. 2*D* and *E*; there was no difference between the mean firing rates of nonstimulated units in laser versus control conditions, $P = 0.5227$, Wilcoxon rank sum test). Notably, during rest, neuron firing rates in response to light stimulation were not different depending on whether the rest sessions were recorded before or after the awake sessions (pre versus post conditions, Wilcoxon rank sum test, $P = 0.85$, across the entire dataset). Although the light-evoked neural signals were stronger in wakefulness compared to rest, signal propagation was significantly weaker in wakefulness compared to rest. Indeed, further examination of the responses of individual units to optogenetic stimulation, starting from the border of the stimulated/nonstimulated units toward the furthest nonstimulated unit (Fig. 2*F*, *Bottom*) revealed that while the increase in population responses significantly decayed as a function of the distance from the border of stimulated sites during wakefulness, elevated firing remained robust across units during rest (Fig. 2*F*; $P < 0.001$, Wilcoxon rank sum test). Individual unit analysis (Fig. 2*F*) was congruent with the population-level analysis (Fig. 2*D* and *E*), showing that firing rates in nonstimulated units in laser trials were elevated in rest relative to control trials ($P < 0.001$, Wilcoxon rank sum test), whereas in wakefulness they decayed to the baseline level of control trials as a function of distance ($P > 0.05$).

Next, we measured the prevalence of laser-induced synchronized On-Off transitions in the stimulated and nonstimulated units. Remarkably, while synchronized spiking activity remained relatively local during wakefulness, it spread vigorously during rest (Fig. 2*B*, *C*, and *G*–*I*). In control trials, the On-Off transition rates calculated by the HMM were not statistically different between stimulated and nonstimulated units ($P > 0.05$; Fig. 2*G*), although, as expected, they were higher in rest compared to wakefulness ($P < 0.01$, χ^2 test). When optogenetic stimulation was applied (laser trials), the On-Off transition rates sharply increased in stimulated units in both behavioral state conditions (Fig. 2*H*; $P < 0.01$, χ^2 test). However, while the induced synchrony remained local to stimulated units during wakefulness, it robustly spread to nonstimulated units during rest (Fig. 2*H*; $P < 0.001$, χ^2 test); that is, whereas the nonstimulated units showed a pronounced decrease in transition rates during wakefulness (a 23-fold decrease from 12.2 to 0.53 transitions/s on average in stimulated versus nonstimulated units; $P < 0.001$, χ^2 test), they showed a relatively smaller decrease during rest (1.4-fold decrease from 17.4 versus 12.8 transitions/s on average in stimulated versus nonstimulated units). During wakefulness, the On-Off transition rates in nonstimulated units in laser trials did not significantly differ from the transition rates in the control ($P > 0.05$, Wilcoxon rank sum test), indicating that the optogenetically induced signals remained local to the stimulated units (Fig. 2*G* and *H*; $P > 0.05$, Wilcoxon rank sum test). However, during rest, the On-Off transition rates in nonstimulated units in laser trials were significantly higher than those in the control condition (91% increase; $P < 0.01$, Wilcoxon rank sum test) to indicate that optogenetic stimulation spread to nonstimulated units (Fig. 2*G* and *H*; $P < 0.001$, Wilcoxon rank sum test).

An alternative measure of synchronized On-Off transitions is the correlation between the temporal profile of the mean population response of directly stimulated units during optogenetic stimulation and the mean population response of nonstimulated units during the same interval (Fig. 2*C*). Notably, this alternative measure of synchrony yielded similar conclusions for our main result (i.e., the correlation between the mean response of stimulated and nonstimulated units in laser trials was significantly higher in rest compared to wakefulness; Fig. 2*C*; $P < 0.001$, Wilcoxon rank sum test). Altogether, these results indicate that laser-induced electrical signals robustly propagate across the cortical column during rest, but not during wakefulness (these results are robust and consistent across animals; *SI Appendix*, Fig. S14).

Controlling the State of Neural Populations Before Optogenetic Stimulation. One key variable that could have influenced the differential propagation of electrical signals across the cortical network is the state of the local population before optogenetic stimulation is applied. Indeed, Fig. 2*G* shows that, as expected, the On-Off transition rate in the control condition was higher in rest compared to wakefulness in the absence of external light stimulation for both stimulated and nonstimulated units ($P < 0.001$, χ^2 test). This could cause optogenetic stimulation to induce a higher rate of On-Off transitions (more synchrony) in stimulated units during rest (Fig. 2*H*), which could potentially increase the degree of signal propagation in nonstimulated units. If that were the case, our results would still stand, but would be simply explained by the higher synchrony state of the local population in rest relative to wakefulness. To ensure that the propagation of optogenetically induced neural signals is not contaminated by naturally occurring synchronous activity during rest, we specifically extracted only those trials in which the population of neurons was desynchronized for at least 1,000 ms before light stimulation in each condition (i.e., zero On-Off transition rate prior to optogenetic stimulation; $P > 0.05$, χ^2 test).

For the trials in which the local population was desynchronized in both brain state conditions (i.e., "Prestim period, all units" condition in Fig. 2*I*, which comprised 44% of trials during rest and 93% of trials during wakefulness), the prestimulation state of the neural population was indistinguishable between wakefulness and rest ($P > 0.05$, χ^2 test, in each session). This led to equal light-induced On-Off transition rates in stimulated units during wakefulness and rest (Stim units; Fig. 2*I*). However, this did not change the extent of propagation of cortical signals across brain states originally reported in Fig. 2*H* ("Non-stim units," Fig. 2*I*); that is, even when the state of the neural population before optogenetic stimulation was identical in both conditions, the spread of light-induced neural signals to adjacent nonstimulated units

during rest remained robust across the entire cortical column, whereas the extent of signal propagation was greatly reduced during wakefulness (Fig. 2*I*; χ^2 test, $P < 0.001$).

To test whether the effects of state-dependent signal propagation were frequency dependent, we varied light frequency between 1, 20, and 35 Hz while laser power and total light exposure were held constant in each condition. For each tested frequency, we calculated the propagation index (PI), defined as the inverse of the difference between the mean firing rates of nonstimulated versus stimulated units in laser trials (low PI values indicate weak propagation, whereas high PI values indicate strong propagation). Across sessions, PI was higher in rest compared to wakefulness for each stimulation frequency (Fig. 2*J*; $P < 0.001$, Wilcoxon rank sum test), indicating that the effects on firing rates were robust irrespective of the frequency of optogenetic stimulation (Fig. 2*J* and *SI Appendix*, Fig. S10). Additionally, for each tested frequency, we calculated the synchrony index (SI), defined as the inverse of the difference between the mean On-Off transitions/s of nonstimulated versus stimulated units in laser trials (low SI values indicate weak propagation, whereas high SI values indicate strong propagation). Across sessions, SI was higher in rest compared to wakefulness for each stimulation frequency (Fig. 2*K*; $P < 0.001$, Wilcoxon rank sum test). Thus, the brain state–dependent signal propagation effects revealed here do not depend on a specific frequency of laser stimulation.

Arousal Influences the Propagation of Light-Induced Neural Signals. We further examined whether trial-by-trial changes in brain state during wakefulness (12) could influence the propagation of neural signals. Previous studies have shown that fluctuations in cortical state covary with global arousal (3, 13) and that a measure of arousal is pupil size (31, 32). Although changes in brain state due to fluctuations in arousal are not as prominent as those between sleep and wakefulness (12), we nonetheless expected differences in the extent of signal propagation. To this end, we grouped the trials in each awake session based on the median pupil size into low arousal (small pupil) and high arousal (large pupil) trials.

Although light-induced synchrony remained mostly local during wakefulness, we found a significant influence of arousal on the extent of signal propagation; that is, we quantified the rate of On-Off state transitions by applying the HMM to subnetworks of fixed size (four units), starting with the stimulated sites and gradually shifting every 100 μm toward the nonstimulated sites (Fig. 2*L*). In states of low arousal (small pupil), there was a higher spread of synchrony (i.e., higher rate of transitions between On and Off states), whereas in the high-arousal state (large pupil), synchrony was strictly limited to the stimulated sites (Fig. 2*M*; Wilcoxon rank sum test, $P < 0.01$). This indicates that contrary to the expectation (3, 8, 13) that higher firing rates observed during the aroused state may enhance the spread of neural signals, alertness actually limits the extent of signal propagation across laminar cortical populations.

State-Dependent Signal Propagation Does Not Depend on the Stimulated . We further examined whether the state-dependent signal propagation that we observed depends on which layer was optogenetically stimulated. In principle, since correlations between neurons are layer dependent [Hansen et al., 2012 (25)], it may be possible that electrical signals could propagate differently depending on laminar identity. We thus repeated the experiments in Fig. 2 by directing laser stimulation to the G, SG, or IG layers while neurons were transiently activated using 10-ms light pulses presented at 20 or 35 Hz for 300 ms, and electrical activity was recorded from all layers simultaneously. In particular, we examined whether or not the lack of signal spread during wakefulness could be due to the laminar location of the subset of neurons we chose to stimulate.

Fig. 3*A* shows the results of one example session in which we stimulated the granular layer during wakefulness—laser stimulation increased the firing rates of granular layer neurons significantly beyond control level to induce local On-Off synchronized transitions (Fig. 3*A*, *Top*; $P < 0.0001$, Wilcoxon rank sum test), reminiscent of the synchronized state during rest. In contrast, the neurons in adjacent nonstimulated layers had a small, but statistically significant, increase in firing rate (Fig. 3*D*; Wilcoxon rank sum test; laser versus control trials in stimulated [G layers]: $P < 0.0001$, nonstimulated [SG and IG layers]: $P < 0.05$). During rest, the light-induced increase in firing rate in the granular layer spread throughout the cortical column to adjacent layers (Fig. 3*A*, *Bottom* and *SI Appendix*, Fig. S16). These results were confirmed by the HMM predictions (i.e., the synchronized state transitions induced in the G layer spread only poorly to adjacent SG and IG layers during wakefulness; Fig. 3*B* and *C*; χ^2 test, $P < 0.001$; control trials represented in Fig. 3*B* and *C*, Bottom; χ^2 test, $P > 0.05$). Across sessions, the weak spread of light-induced population spiking activity during wakefulness was observed regardless of which layer was optogenetically stimulated (Fig. 3*E*). In contrast to wakefulness, the light-induced neural signals during rest (measured by the On-Off transition rate) robustly spread to adjacent nonstimulated layers across the cortical column (Fig. 3*F*; i.e., the On-Off transition rates in nonstimulated layers returned to baseline [control trials, $P > 0.05$]) in wakefulness but remained significantly elevated in rest (79% increase, laser versus control; $P < 0.001$, Wilcoxon rank sum test). Altogether, these results indicate that layer identity is not a confound restricting the spread of neural activity across the laminar circuit during wakefulness, thereby confirming our findings that brain state modulates signal propagation across the cortical column independent of layer identity.

Population Coupling Explains the Brain-State Dependency of Signal Propagation. What mechanism could underlie the influence of global brain state on the degree of propagation of spiking activity across laminar networks? Since the spread of neural signals was limited during wakefulness but significantly less restricted during rest, we reasoned that the strength of functional connectivity across columnar neurons may exhibit state dependency. We thus computed the strength of coupling between individual neurons and their local population and hypothesized that coupling would be weak during wakefulness but strong during rest. Notably, population coupling is a correlate of synaptic connectivity [i.e., the population coupling of a neuron provides an estimate of the number of synapses received by a neuron from its neighbors (33)].

To quantify population coupling, we computed spike-triggered population rates by correlating the spike train of each neuron with the summed activity of the neural population (excluding the neuron being examined; Fig. 4*A*). Population coupling was remarkably higher in rest compared to wakefulness (Fig. 4*B*, *Left*; Wilcoxon rank sum test, $P < 0.01$), and the degree of state modulation was more pronounced during laser stimulation (Fig. 4*B*, *Right*; Wilcoxon rank sum test, $P < 0.001$). Neurons that were weakly coupled to their neighboring neurons during wakefulness became strongly coupled with their neighbors during rest. Thus, increased coupling between individual neurons and their local population allows a greater spread of synchronous activity during rest, whereas weaker coupling during wakefulness limits signal propagation (Figs. 2*A* and 3*A*). We further asked whether the difference in population coupling between wakefulness and rest is maintained when neurons are in a desynchronized wake-like state prior to light stimulation (as in Fig. 2*I*). However, when we

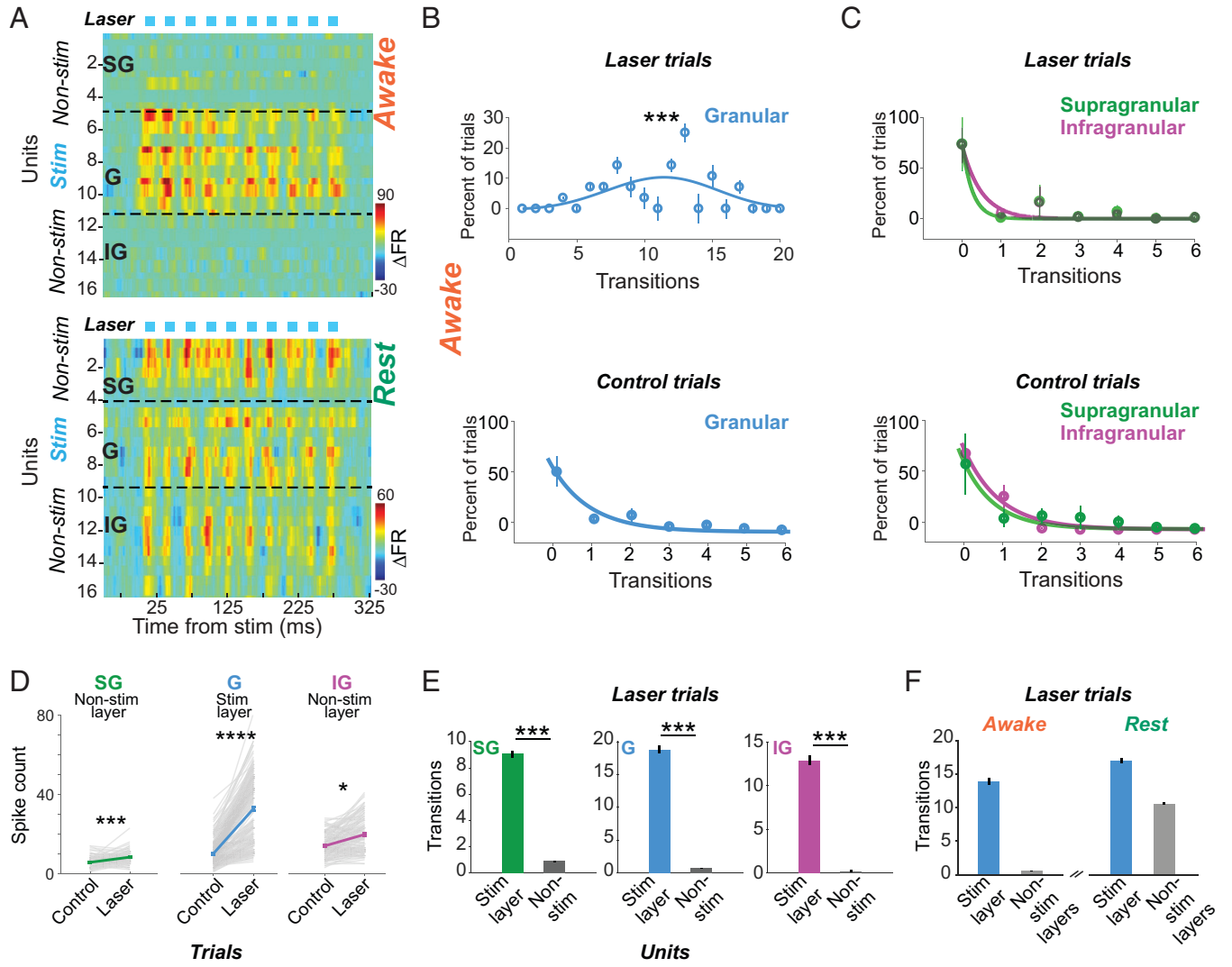

Fig. 3. Optogenetically induced On-Off states remain local during wakefulness. (*A*) Difference in firing rates (ΔFR) between "light stimulation" and control trials across all single units in an example session. Laser stimulation was performed at 35 Hz using 10-ms pulses for 300 ms in wakefulness (*Top*) and rest (*Bottom*). Optogenetically induced On (high FR) and Off (low FR) states in the granular (G) layer with concurrent recordings from nonstimulated SG and IG layers. (*B* and *C*) *Top:* Histogram of rate of transitions between On and Off states across all wakefulness sessions. Transition rate in G (stimulated, blue) compared to SG (nonstimulated, green) and IG (nonstimulated, magenta) for all sessions (G versus SG, ***$P < 0.001$; G versus IG, ***$P < 0.001$, χ^2 test, $n = 5$ sessions). Error bars represent SEM. *Bottom:* Histogram of rate of transitions between On and Off states in control trials. Transition rate in G (blue) compared to SG (green) and IG (magenta) for all wakefulness sessions (G versus SG, $P > 0.05$; G versus IG, $P < 0.05$, χ^2 test, $n = 5$ sessions). Error bars represent SEM. (*D*) Spike counts across sessions in laser trials compared to control trials for each layer in wakefulness. Gray lines represent trials; solid bars represent mean spike counts. Error bars represent SEM. (G laser versus G control, ****$P < 0.0001$; SG laser versus SG control, ***$P < 0.001$; IG laser versus IG control, *$P < 0.05$, Wilcoxon rank sum test, $n = 5$ sessions). (*E*) Transitions/s plotted as mean and SEM during stimulation of SG, G, and IG layers in wakefulness (transition rate in Stim layer versus Non-stim layers. ***$P < 0.001$, Wilcoxon rank sum test, $n = 7$ sessions). (*F*) On-Off transition rates plotted as mean and SEM during laser stimulation for stimulated and nonstimulated layers in awake and rest conditions (transition rate in awake versus rest Non-stim layers; $P < 0.001$, Wilcoxon rank sum test, $n = 13$ sessions). Non-stim, nonstimulated; Stim, stimulated.

selected only the trials in which population activity was indistinguishable between wakefulness and rest 1,000 ms before optogenetic stimulation ($P = 0.59$, Wilcoxon rank sum test), we found that coupling during laser stimulation remained significantly higher in rest compared to wakefulness ($P < 0.0001$, bootstrap test). Altogether, these analyses indicate that population coupling changes as a function of brain state such that the input connection strength dynamically shifts between wakefulness and rest—an underlying mechanism explaining how brain state modulates signal propagation in laminar circuits.

Discussion

Using a combination of multielectrode laminar recordings and optogenetics, we found that the propagation of electrical signals is strongly influenced by global brain state. Following the optogenetic induction of synchronized activity in a subset of neurons, we found a significantly larger spread of neural signals during rest compared to wakefulness. Remarkably, even when we strictly controlled for the state of the neural population before light stimulation, synchronous signals robustly spread during rest but remained local in wakefulness. Furthermore, a global variable controlling the awake state, arousal, was inversely correlated with the spread of neuronal signals. The almost total lack of synchronized fluctuations across layers during wakefulness when On-Off state transitions are optogenetically induced in one layer is surprising given the presence of strong interlayer connections mediating information transfer (17, 19, 20, 34). This suggests that during wakefulness there is a remarkable degree of independence of individual layers, which may act as independent functional units during sensory processing (25).

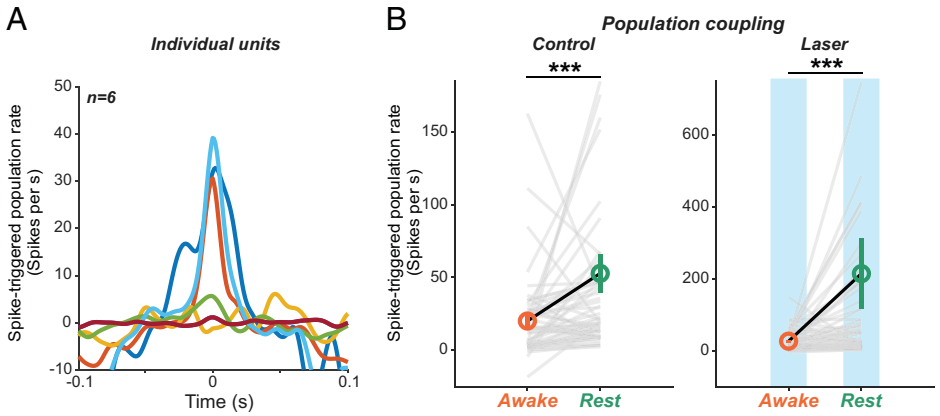

Fig. 4. State-dependent changes in population coupling. (*A*) Spike-triggered population rate for six example neurons. (*B*) Spike-triggered population rate across sessions in wakefulness compared to rest for control and laser conditions. Gray lines represent individual units, and circles represent the means. Error bars represent SEM (control awake versus rest, ***$P < 0.001$; laser awake versus rest, ***$P < 0.001$, Wilcoxon rank sum test, $n = 12$ sessions).

Mechanistically, our results can be explained by the state-dependent coupling between individual neurons and local population activity. Indeed, neurons were more coupled to their neighbors during rest compared to wakefulness, and population coupling controlled signal propagation. An additional mechanism could be state-dependent modulation of the balance between local excitation and inhibition (35, 36). Theoretically, it has been proposed that the excitation-inhibition (E/I) ratio impacts fluctuations in local populations, including low-frequency synchrony and correlations (25, 37, 38). Furthermore, experiments in rodents have revealed that sleep regulates cortical E/I balance (39), with inhibitory interneurons responding only weakly during slow-wave sleep and maximally during rapid eye movement sleep and wakefulness (9, 40). We confirmed in our data set that the E/I ratio (based on functionally defined cell types; *SI Appendix*, Fig. S11) is significantly higher in rest compared to wakefulness (*SI Appendix*, Fig. S11). This raises the possibility that a decrease in E/I ratio from rest to wakefulness, along with a decrease in population coupling, contributes to restricting the propagation of cortical population activity (41–43).

What could be the functional significance of the state-dependent propagation of neural signals revealed here? The optimal network state during wakefulness is the desynchronized mode. Indeed, desynchronized cortical activity has been shown to be important for sensory coding and perception (12, 25, 44) (i.e., when cells are desynchronized, populations of neurons encode more information to increase perceptual accuracy). However, how electrical signals propagate along the cortical column in different brain states has remained unknown. The weaker signal propagation across the cortical column during wakefulness observed here could constitute an efficient "noise-reduction" mechanism that operates by blocking the propagation of electrical signals elicited by distractor stimuli. Indeed, since the generation of action potentials is metabolically expensive, the brain must prevent weak, irrelevant stimuli from eliciting spiking activity in target neurons.

In contrast to wakefulness, rest is associated with significantly stronger coupling of individual neurons to local population activity (cf. Fig. 4), which contributes to enhanced signal propagation. This dynamic shift in population coupling from wakefulness to rest may be a mechanism by which cortical networks undergo synchronicity, a fundamental phenomenon required for the brain's daily maintenance [e.g., upscaling/downscaling synaptic connections and eliminating metabolic waste (28, 42, 45)]. Furthermore, strong coupling during rest would be advantageous to ensure the maintenance of endogenously generated Up and Down states, which, although ubiquitously observed during slow-wave sleep (28), remain poorly understood.

Overall, we found that cells are more coupled during rest (higher population coupling), and hence the light-evoked action potentials have a higher probability of being transmitted across layers. In contrast, cells are significantly less coupled during wakefulness, and this reduces the transmission probability of light-evoked action potentials across layers. We also showed that this shift occurs across a continuum of brain states—when the animal goes from high arousal to low arousal (drowsiness) to rest. These findings may suggest a refinement of the conclusions of causal manipulation studies attempting to influence neuronal responses and behavior (30, 46–48), as well as of current computational models of perception assuming robust signal propagation across cortical layers and areas (49–51). However, this idea has been taken for granted in optogenetic and electrical stimulation studies in behaving animals (47, 52, 53). That is, signal propagation is generally assumed, but uncontrolled for. We showed that brain state strongly influences how far signals travel in neocortex. Thus, studies relying on causal optogenetic or electrical stimulation methodology should control for the state of the brain at the time of stimulation, as one might observe stronger effects in the drowsy relative to the alert state (cf. Fig. 2*M*). The brain state of the animal could complicate the interpretation of causal stimulation manipulations, popular in systems neuroscience and brain-machine interface studies (30, 46, 53–57). This idea is consistent with a previous study (58) showing that electrical stimulation in the anesthetized, but not awake, state leads to activation at post-synaptic sites in V1, but suppression at synaptically later sites in the extrastriate cortex. However, one caveat of our findings is that optogenetic activation does not mimic the pattern of neural activity observed under normal visual stimulation conditions. In addition, technical limitations prevented us from varying light intensity (but not frequency); hence, we were unable to evoke the wide range of responses that one would normally expect during natural vision. Despite all these limitations, optogenetic stimulation allowed us to probe the degree of signal propagation in columnar circuits in different brain states and thus discover, within our experimental framework, that propagation is stronger during rest.

Taken together, our findings provide a key insight into the brain state–dependent propagation of neural signals across columnar circuits and its functional significance. Revealing the neural network underpinnings of how and why the brain switches from an asynchronous to a synchronous state may pave the way for new approaches to investigating the aberrant synchrony observed

in a myriad of neuropsychiatric disorders such as epilepsy, Alzheimer disease, schizophrenia, and autism (45, 59). Given the similarities of columnar microcircuitry associated with different sensory modalities (16, 17, 60–62), the brain-state control of dynamics and spread of cortical spiking activity revealed here could constitute a general principle of signal propagation across sensory cortical populations.

Methods

Detailed methods are provided in the *SI Appendix*. All experiments were performed in accordance with protocols approved by NIH Guidelines for the Care and Use of Animals for Experimental Procedures and approved by the Institutional Animal Care and Use Committee at the University of Texas Health Science Center at Houston. Monkeys were trained for 3 to 4 months on visual fixation and contrast detection. After learning, a recording chamber (17-mm inner diameter) for single-unit multiple electrode recording was cemented over areas V1 and V4 (according to the MRI map). A total of 75 sessions and 1,407 units in area V1 were recorded from three rhesus monkeys (*Macaca mulatta*): W, C, and T. Overall, we recorded from 1,920 cells across the layers of V1 in three monkeys ($n = 95$ sessions across all behavioral states). We recorded 789 V1 units in the task condition, 608 V1 units in the fixation (no stimulus) condition, and 523 V1 units in the rest condition. An additional 54 sessions and 856 units were recorded in area V4 (*SI Appendix*, Figs. S3–S8). For area V4, we recorded from 1,712 cells across the layers of V4 in two monkeys ($n = 108$ sessions across all behavioral states). We recorded 856 V4 units in the task condition, 600 V4 units in the fixation (no stimulus) condition, and 256 V4 units in the rest condition.

Electrophysiological Recordings. Neuronal activity was recorded using laminar probes with 16 to 24 equally spaced contacts at 100 μm (U-Probe, Plexon) advanced into the brain using a NAN drive system (Plexon) attached to the recording chamber. All penetrations were perpendicular to the cortical surface and initiated at the same depth relative to surface. We recorded spiking and LFP signals using a Multichannel Acquisition Processor System (Plexon). LFP power ratio (PR) was computed from the LFP power in the low- (0.5- to 10-Hz) and high- (30- to 80-Hz) frequency bands, PR = (P10 − P80)/P10, where P10 is the spectral power in the 0.5- to 10-Hz range, and P80 is the spectral power in the 30- to 80-Hz range. LFP analysis confirmed the behavioral state of the animal in each session (12). Cortical layers were identified using the current source density (CSD) analysis (25). We computed the CSD by using the second spatial derivative of LFP time series across equally spaced laminar contacts using the inverse current source density (iCSD) toolbox for MATLAB. The granular layer was identified by finding the earliest current sink, measured by nanoampere per cubic millimeter. Channels located in the primary sink were assigned to the granular layer, those above the sink were assigned to the supragranular layer, and channels below the sink were assigned to the infragranular layer (25).

Eye Movement Monitoring. To ensure fixation, eye position was constantly monitored by an eye tracker operating at 1 KHz (EyeLink II; SR Research), whose gains were adjusted to be linear for horizontal and vertical eye deflections. Eye position was calibrated at the beginning of each session using a five-point calibration procedure. On each trial, monkeys were trained to fixate on a 0.2-degree (deg) dot at the center of the screen within a rectangular 1- to 2-deg window. Microsaccades were analyzed every 10 ms by using a vector velocity threshold of 10 deg/s (i.e., a 0.1-deg eye movement between consecutive 10-ms intervals).

Wakefulness and Rest Experiments. During wakefulness, monkeys performed passive fixation (no stimulus) and contrast detection. During rest, monkeys were in a dark room for 20 to 45 min. During wakefulness and rest sessions, we recorded single and multiunit activity from area V1 (57 sessions; similar experiments were performed in area V4 in 54 sessions; e.g., *SI Appendix*, Figs. S1, S3*B*, S4, S5, S6*B*, S7, and S8*B*). We measured the dynamics of laminar population activity for a period of 1 s across trials during wakefulness and rest and focused on comparing rest and wakefulness in the absence of visual stimulation (during passive fixation and during the task).

Passive fixation. Monkeys fixated on a 0.1-deg central point presented on a 19-inch CRT monitor(Dell, 60-Hz refresh rate) on a dark background in a dark room. Fixation was maintained within a 1-deg window for 1,000 ms in the absence of sensory stimulation. Each session consisted of 120 to 480 trials. We recorded 3,840 trials across 32 sessions (608 units).

Task. Monkeys performed a contrast detection task using gray-scale sinusoidal gratings of luminance-varying contrasts generated using Psychophysics Toolbox 75 and presented binocularly on a 19-inch CRT video monitor (Dell, 60-Hz refresh rate) on a dark background in a dark room. While monkeys fixated, stimuli with a diameter of 2 to 3 deg were displayed at 2- to 4-deg eccentricity. The location and size of stimuli covered the multiple receptive fields of the cells recorded (*SI Appendix*, Fig. S1). Stimuli had a fixed spatial frequency (1.7 cpd) and were displayed for 300 ms (starting 450 to 1,000 ms after fixation onset), followed by a 1.1-s delay ("blank" screen). In each experiment, stimuli could have one of four different luminance contrasts and were present on 50% of trials. At the end of the delay interval, monkeys were required to signal the presence of the stimulus by releasing the lever or maintaining contact if no stimulus was displayed.

Rest. Each session consisted of 360 to 720 total trials. A total of 11,520 trials across 31 sessions were recorded. A rest session was considered valid if (i) the monkey's eyes were closed for >85% of total session duration and (ii) the LFP PR was significantly higher (Wilcoxon rank sum test, $P < 0.05$) in rest compared to wakefulness (fixation and task). A total of 31 rest sessions across three monkeys met our criteria, from which we recorded 523 units.

HMM Analysis. We fit an HMM to our spiking data as described previously (23). Briefly, multi-unit and single-unit summed spiking data were binned every 10 ms, and the HMM, which assumes that spikes are generated via a Poisson process, was fitted to spiking data to identify two states (On and Off states) and the transition probabilities between these states using the hmmtrain function in MATLAB R2017b. The model was trained on 50% of the dataset and tested on the remaining 50%. The model output was analyzed using the hmmviterbi function in MATLAB R2017b, which utilizes the Viterbi algorithm to classify spiking data into the two states for all time points. As a control, the HMM was trained on shuffled data (by shuffling spike times for each unit). The final output (i.e., the output of the model trained on the original data subtracted from the output of the model trained on shuffled data) was analyzed to determine the average firing rates in the On and Off states and their durations. The HMM was fitted to the population activity of single and multiunit activity recorded across a cortical column, and the model was fitted to each session. To test for robustness, we repeated the analysis by fitting the model across all sessions, and the results did not significantly differ.

Optogenetics Experiments. ChR2 was expressed specifically in V1 excitatory cells using a lentiviral vector as described previously (30). High-titer (>10^9 IU/mL) purified lentivirus was obtained from the University of North Carolina Gene Therapy Center Vector Core. Optogenetic stimulation was achieved using a 100 mega watt (mW) transistor-transistor-logic (TTL)-controlled Diode-Pumped Solid-State (DPSS) blue (473-nm) laser (RGBLase) coupled to a 200-μm optical fiber. The end of the fiber was inserted into a 356-μm stainless steel cannula for stability and mounted on the NAN Microdrive. Light intensity at the tip of the cannula was ≤10 mW/mm^2 (Coherent Lasermate power meter) so as to target ∼400 μm of brain area [equivalent to the anatomical measurement of a cortical layer (25)]. The optic fiber and electrodes were mounted separately and could be manipulated independently; they were positioned to minimize the distance between the optical fiber tip and the probe, with the devices often touching at the target depth (i.e., the middle of the target cortical layer as analyzed using CSD). For example, if the granular layer spanned channels 4 through 8 (400 to 800 μm), we inserted the optic fiber to a depth of 600 μm. After the optic fiber and a recording electrode were advanced into the cortex and reached the injection depth, optical stimulation of the neurons was achieved by delivering 10-ms light pulses at 1 Hz (1 cycle; 2 sessions), 20 Hz (10 or 15 cycles; 4 sessions), or 35 Hz (10 cycles; 16 sessions). To examine signal propagation in different brain states, a total of 18 sessions (200 to 720 total trials) were performed with 342 V1 units recorded in monkeys W and C. Wakefulness and rest sessions were either arranged in rest-awake-rest or awake-rest-awake blocks on a given day. On each stimulation trial, the laser was triggered 300 ms after the monkey acquired fixation (average inter-trial interval was 14 s). Optogenetic stimulation and control (no laser) trials were matched in number and were randomly and evenly distributed across trials. During rest, the same optogenetic stimulation protocol was repeated while lights were turned off (stimulation and no-stimulation trials were randomly interleaved). The duration and number of light stimulation and control trials were identical for wakefulness and rest conditions.

Population Coupling. Population coupling was computed by calculating the cross-correlation between the smoothed firing rate of a neuron and the spike-triggered average of the population (stPR) (33). The population rate used for stPR computation for an individual unit excluded the spikes of that unit. The population rate was computed by accumulating spiking activity of all (multi/single) units with 1-ms resolution and smoothing the resulting vector with a Gaussian of half-width 12 ms (33). The baseline level of each stPR was subtracted. For individual units, the firing rate of a unit was computed with 1-ms resolution while smoothing the resulting vector with a Gaussian of half width of $12/\sqrt{2}$ ms.

Statistical Analysis. We used the Wilcoxon rank sum test for rest and wakefulness comparisons. In other cases, we used the χ^2 test and Pearson correlation for significance analysis. We applied the Holm-Bonferroni correction wherever multiple comparisons were performed. All differences reported in spontaneous and optogenetically induced state transitions were significant in each individual monkey ($P < 0.05$, Wilcoxon rank sum). Furthermore, there were no significant differences between monkeys ($P > 0.05$, χ^2 test).

Data and Code Availability. The data and custom code that support the findings from this study are openly available via email to valentin.dragoi@uth.tmc.edu. All other study data are included in the article and/or *SI Appendix*.

ACKNOWLEDGMENTS. We thank S. Eagleman and S. Pojoga for contributions to this project and S. Nigam and M.I. Chelaru for helpful discussions and comments on the manuscript. This work was supported by NIH Grant No. R01EY026156.

1. C. Y. Li, M. M. Poo, Y. Dan, Burst spiking of a single cortical neuron modifies global brain state. *Science* **324**, 643–646 (2009).
2. K. D. Harris, A. Thiele, Cortical state and attention. *Nat. Rev. Neurosci.* **12**, 509–523 (2011).
3. M. J. McGinley *et al.*, Waking state: Rapid variations modulate neural and behavioral responses. *Neuron* **87**, 1143–1161 (2015).
4. J. F. A. Poulet, C. C. H. Petersen, Internal brain state regulates membrane potential synchrony in barrel cortex of behaving mice. *Nature* **454**, 881–885 (2008).
5. M. M. Steriade, R. McCarley, *Brain Control of Wakefulness and Sleep* (Springer US, 2005).
6. D. S. Greenberg, A. R. Houweling, J. N. D. Kerr, Population imaging of ongoing neuronal activity in the visual cortex of awake rats. *Nat. Neurosci.* **11**, 749–751 (2008).
7. J. T. Daley, R. S. Turner, A. Freeman, D. L. Bliwise, D. B. Rye, Prolonged assessment of sleep and daytime sleepiness in unrestrained *Macaca mulatta*. *Sleep* **29**, 221–231 (2006).
8. C. M. Niell, M. P. Stryker, Modulation of visual responses by behavioral state in mouse visual cortex. *Neuron* **65**, 472–479 (2010).
9. N. Niethard *et al.*, Sleep-stage-specific regulation of cortical excitation and inhibition. *Curr. Biol.* **26**, 2739–2749 (2016).
10. A. S. Ecker *et al.*, State dependence of noise correlations in macaque primary visual cortex. *Neuron* **82**, 235–248 (2014).
11. J. F. Mitchell, K. A. Sundberg, J. H. Reynolds, Differential attention-dependent response modulation across cell classes in macaque visual area V4. *Neuron* **55**, 131–141 (2007).
12. C. B. Beaman, S. L. Eagleman, V. Dragoi, Sensory coding accuracy and perceptual performance are improved during the desynchronized cortical state. *Nat. Commun.* **8**, 1308 (2017).
13. M. Vinck, R. Batista-Brito, U. Knoblich, J. A. Cardin, Arousal and locomotion make distinct contributions to cortical activity patterns and visual encoding. *Neuron* **86**, 740–754 (2015).
14. K. Brodmann, *Vergleichende Lokalisationslehre der Grosshirnrinde in ihren Prinzipien dargestellt auf Grund des Zellenbaues* (Barth, 1909).
15. D. H. Hubel, T. N. Wiesel, Receptive fields and functional architecture of monkey striate cortex. *J. Physiol.* **195**, 215–243 (1968).
16. R. J. Douglas, K. A. C. Martin, Neuronal circuits of the neocortex. *Annu. Rev. Neurosci.* **27**, 419–451 (2004).
17. K. D. Harris, G. M. G. Shepherd, The neocortical circuit: Themes and variations. *Nat. Neurosci.* **18**, 170–181 (2015).
18. J. A. Hirsch, L. M. Martinez, Laminar processing in the visual cortical column. *Curr. Opin. Neurobiol.* **16**, 377–384 (2006).
19. J. J. Nassi, E. M. Callaway, Parallel processing strategies of the primate visual system. *Nat. Rev. Neurosci.* **10**, 360–372 (2009).
20. N. T. Markov *et al.*, Anatomy of hierarchy: Feedforward and feedback pathways in macaque visual cortex. *J. Comp. Neurol.* **522**, 225–259 (2014).
21. M. V. Sanchez-Vives, D. A. McCormick, Cellular and network mechanisms of rhythmic recurrent activity in neocortex. *Nat. Neurosci.* **3**, 1027–1034 (2000).
22. M. A. Smith, X. Jia, A. Zandvakili, A. Kohn, Laminar dependence of neuronal correlations in visual cortex. *J. Neurophysiol.* **109**, 940–947 (2013).
23. T. A. Engel *et al.*, Selective modulation of cortical state during spatial attention. *Science* **354**, 1140–1144 (2016).
24. P. Lakatos, C. M. Chen, M. N. O'Connell, A. Mills, C. E. Schroeder, Neuronal oscillations and multisensory interaction in primary auditory cortex. *Neuron* **53**, 279–292 (2007).
25. B. J. Hansen, M. I. Chelaru, V. Dragoi, Correlated variability in laminar cortical circuits. *Neuron* **76**, 590–602 (2012).
26. N. Shahidi, A. R. Andrei, M. Hu, V. Dragoi, High-order coordination of cortical spiking activity modulates perceptual accuracy. *Nat. Neurosci.* **22**, 1148–1158 (2019).
27. L. Baum, T. Petrie, G. Soules, N. Weiss, A maximization technique occurring in the statistical analysis of probabilistic functions of Markov chains. *Ann. Math. Statist.* **41**, 164–171 (1970).
28. G. Tononi, C. Cirelli, Sleep function and synaptic homeostasis. *Sleep Med. Rev.* **10**, 49–62 (2006).
29. J. A. Cardin *et al.*, Driving fast-spiking cells induces gamma rhythm and controls sensory responses. *Nature* **459**, 663–667 (2009).
30. A. R. Andrei, S. Pojoga, R. Janz, V. Dragoi, Integration of cortical population signals for visual perception. *Nat. Commun.* **10**, 3832 (2019).
31. S. L. Merritt, H. C. Schnyders, M. Patel, R. C. Basner, W. O'Neill, Pupil staging and EEG measurement of sleepiness. *Int. J. Psychophysiol.* **52**, 97–112 (2004).
32. S. Joshi, Y. Li, R. M. Kalwani, J. I. Gold, Relationships between pupil diameter and neuronal activity in the locus coeruleus, colliculi, and cingulate cortex. *Neuron* **89**, 221–234 (2016).
33. M. Okun *et al.*, Diverse coupling of neurons to populations in sensory cortex. *Nature* **521**, 511–515 (2015).
34. C. D. Gilbert, T. N. Wiesel, Clustered intrinsic connections in cat visual cortex. *J. Neurosci.* **3**, 1116–1133 (1983).
35. N. Dehghani *et al.*, Dynamic balance of excitation and inhibition in human and monkey neocortex. *Sci. Rep.* **6**, 23176 (2016).
36. M. Rudolph, M. Pospischil, I. Timofeev, A. Destexhe, Inhibition determines membrane potential dynamics and controls action potential generation in awake and sleeping cat cortex. *J. Neurosci.* **27**, 5280–5290 (2007).
37. A. Renart *et al.*, The asynchronous state in cortical circuits. *Science* **327**, 587–590 (2010).
38. H. Markram *et al.*, Interneurons of the neocortical inhibitory system. *Nat. Rev. Neurosci.* **5**, 793–807 (2004).
39. M. C. D. Bridi *et al.*, Daily oscillation of the excitation-inhibition balance in visual cortical circuits. *Neuron* **105**, 621–629.e4 (2020).
40. B. Haider, M. Häusser, M. Carandini, Inhibition dominates sensory responses in the awake cortex. *Nature* **493**, 97–100 (2013).
41. Y. Chagnac-Amitai, B. W. Connors, Horizontal spread of synchronized activity in neocortex and its control by GABA-mediated inhibition. *J. Neurophysiol.* **61**, 747–758 (1989).
42. M. Patel, B. Joshi, Decoding synchronized oscillations within the brain: Phase-delayed inhibition provides a robust mechanism for creating a sharp synchrony filter. *J. Theor. Biol.* **334**, 13–25 (2013).
43. M. Xue, B. V. Atallah, M. Scanziani, Equalizing excitation-inhibition ratios across visual cortical neurons. *Nature* **511**, 596–600 (2014).
44. D. A. Gutnisky, V. Dragoi, Adaptive coding of visual information in neural populations. *Nature* **452**, 220–224 (2008).
45. P. J. Uhlhaas, W. Singer, Neural synchrony in brain disorders: Relevance for cognitive dysfunctions and pathophysiology. *Neuron* **52**, 155–168 (2006).
46. C. R. Fetsch *et al.*, Focal optogenetic suppression in macaque area MT biases direction discrimination and decision confidence, but only transiently. *eLife* **7**, 1–23 (2018).
47. S. H. Lee *et al.*, Activation of specific interneurons improves V1 feature selectivity and visual perception. *Nature* **488**, 379–383 (2012).
48. C. D. Salzman, K. H. Britten, W. T. Newsome, Cortical microstimulation influences perceptual judgements of motion direction. *Nature* **346**, 174–177 (1990).
49. A. Pouget, P. Dayan, R. Zemel, Information processing with population codes. *Nat. Rev. Neurosci.* **1**, 125–132 (2000).
50. P. Dayan, L. F. Abbott, *Theoretical Neuroscience : Computational and Mathematical Modeling of Neural Systems* (The MIT Press, 2001).
51. D. B. Rubin, S. D. Van Hooser, K. D. Miller, The stabilized supralinear network: A unifying circuit motif underlying multi-input integration in sensory cortex. *Neuron* **85**, 402–417 (2015).
52. C. R. Fetsch, R. Kiani, W. T. Newsome, M. N. Shadlen, Effects of cortical microstimulation on confidence in a perceptual decision. *Neuron* **83**, 797–804 (2014).
53. M. Jazayeri, Z. Lindbloom-Brown, G. D. Horwitz, Saccadic eye movements evoked by optogenetic activation of primate V1. *Nat. Neurosci.* **15**, 1368–1370 (2012).
54. D. C. Millard, C. J. Whitmire, C. A. Gollnick, C. J. Rozell, G. B. Stanley, Electrical and optical activation of mesoscale neural circuits with implications for coding. *J. Neurosci.* **35**, 15702–15715 (2015).
55. J. E. O'Doherty *et al.*, Active tactile exploration using a brain-machine-brain interface. *Nature* **479**, 228–231 (2011).
56. E. S. Boyden, F. Zhang, E. Bamberg, G. Nagel, K. Deisseroth, Millisecond-timescale, genetically targeted optical control of neural activity. *Nat. Neurosci.* **8**, 1263–1268 (2005).
57. O. Yizhar, L. E. Fenno, T. J. Davidson, M. Mogri, K. Deisseroth, Optogenetics in neural systems. *Neuron* **71**, 9–34 (2011).
58. N. K. Logothetis *et al.*, The effects of electrical microstimulation on cortical signal propagation. *Nat. Neurosci.* **13**, 1283–1291 (2010).
59. P. J. Uhlhaas, W. Singer, Abnormal neural oscillations and synchrony in schizophrenia. *Nat. Rev. Neurosci.* **11**, 100–113 (2010).
60. V. B. Mountcastle, The columnar organization of the neocortex. *Brain* **120**, 701–722 (1997).
61. H. F. Song, H. Kennedy, X.-J. Wang, Spatial embedding of structural similarity in the cerebral cortex. *Proc. Natl. Acad. Sci. U.S.A.* **111**, 16580–16585 (2014).
62. D. H. Hubel, T. N. Wiesel, Uniformity of monkey striate cortex: A parallel relationship between field size, scatter, and magnification factor. *J. Comp. Neurol.* **158**, 295–305 (1974).